Materials Science-Poland, 40(4), 2022, pp. 43-53
http://www.materialsscience.pwr.wroc.pl/
DOI: 10.2478/msp-2022-0045

$NiTiO_3/MnFe_2O_4$ ferrite composites: synthesis, optical, ferroelectric and magnetic properties

Dang Thi Thom[1], Nguyen Hoang Tuan[1], Tran Vu Diem Ngoc[2], Nguyen Tuyet Nga[1], Nguyen Thanh Phuong[1], Dang Duc Dung[1], Do Thi Kim Thoa[1], Luong Huu Bac[1,*]

[1]School of Engineering Physics, Ha Noi University of Science and Technology, Hanoi, Vietnam
[2]School of Materials Science and Engineering, Ha Noi University of Science and Technology, Hanoi, Vietnam

This work reported the successful synthesis of ilmenite-spinel $(1-x)NiTiO_3$-$xMnFe_2O_4$ (x = 0, 0.05 and 0.10) composites by a simple sol-gel method. Phase formation of composites was analyzed by the X-ray diffraction method. All the synthesized samples formed diphasic ilmenite-ferrite composites without any trace of impurity or intermediate phase. The optical properties of synthesized composites were characterized by diffuse reflectance UV–visible spectroscopy. $MnFe_2O_4$ phase modified the optical band gap of $NiTiO_3$ material and shifted its optical bandgap value toward lower energy. Ferroelectric and magnetic hysteresis loops were investigated at room temperature. The hysteresis loops indicated the typical ferromagnetic and ferroelectric nature of all composites at room temperature. In P-E loops, the remanent polarization (P_r) and saturation polarization (P_s) showed a slight increase in the sample with 5% $MnFe_2O_4$ phase addition. However, the lossy *P-E* loop was observed in the sample with the addition of 10% $MnFe_2O_4$. The presence of ferrite $MnFe_2O_4$ phase in $NiTiO_3$ material enhanced the magnetic properties of $NiTiO_3$ at room temperature. The *M-H* loops of $NiTiO_3$-$MnFe_2O_4$ composites presented a ferromagnetic behavior with a dramatic increase in saturation magnetization with an increase of ferrite phase addition.

Keywords: *Sol-gel processes; $NiTiO_3$, $MnFe_2O_4$, composites, ferroelectric properties, magnetic properties*

1. Introduction

The multiferroic ceramics are materials in which both ferromagnetic and ferroelectric behaviors occur simultaneously and both magnetic and electric properties can be controlled by changing the applied electric and/or magnetic fields. Magnetic fields can affect the electrical polarization and conversely an electrical field can affect the magnetization. However, the coexistence of both electric and magnetic properties in a single-phase material is almost mutually exclusive because the mechanism of the occurrence of combined ferroelectric and ferromagnetic properties is unfavorable, which limits the practical applications [1]. That is why numerous researchers have been looking recently for alternative ways to integrate two or more magnetic and electric phases in one material that can obtain ferroelectric and ferromagnetic ordering in the material [2, 3]. A composite of magnetic and electric phases is expected to have relatively strong magneto-electric coupling between ferroic characteristics.

$NiTiO_3$ (NTO) is a material that belongs to the family with formula $ATiO_3$, in which A is a transition metal such as Fe, Mn, Co, Ni, and so on. It is of particular interest because of its optical, electrical, and magnetic properties. $NiTiO_3$ is an semiconductor with a bandgap value ranging from 2.2 eV-2.8 eV [4] and is antiferromagnetic with a Neel temperature about $-251 \div -252^{\circ}C$ [5]. Previous reports showed that $NiTiO_3$ exhibited ferroelectric characteristics at room temperatures [6–8]. Generally, magnetic properties of $NiTiO_3$ ceramic can be changed by metal transition dopants [9–11]. Doping with transition metal can induce ferromagnetic properties due to induction of oxygen vacancies [9]. Lenin et al. reported that Fe doping in the $NiTiO_3$ lattice can enhance magnetic properties [11]. In contrast to this result, Tursun et al. found that the Zn, Cu, Mn, Co, and Fe doped $NiTiO_3$ sample exhibited ferroelectric properties and the Fe,

* E-mail: bac.luonghuu@hust.edu.vn

Cu, Zn doped $NiTiO_3$ samples with 5 mol.% doping had ferromagnetic properties [10]. However, the magnetic saturation (M_s) and remanent magnetization (M_r) values of doped $NiTiO_3$ samples were small and caused a reduction in ferroelectric properties of $NiTiO_3$ material.

Manganese ferrite ($MnFe_2O_4$-MFO) ceramic is a spinel ferrite material which is one of the important magnetic oxides, with specific physical and chemical properties [12, 13]. $MnFe_2O_4$ has soft magnetic properties with low coercivity, high magnetic permeability, and moderate saturation magnetization [14, 15]. This material can be employed as a magnetic phase in composite materials to enhance magnetic properties. Many studies previously reported on composites of ferroelectric materials, such as $BiFeO_3$, $BaTiO_3$, $PbTiO_3$ and spinel-type ferrites such as $MnFe_2O_4$, $CoFe_2O_4$ [16–18]. Jain et al. reported that $Ba_{0.83}Ca_{0.10}Sr_{0.07}TiO_3$-$MnFe_2O_4$ composites showed a slight drop in dielectric, piezoelectric, and ferroelectric properties, with $MnFe_2O_4$ addition. However, there is a significant increase in magnetic and magneto-electric properties [19]. Pachari et al. studied the effects of several types of ferrite ($ZnFe_2O_4$, $CoFe_2O_4$ and $Co_{0.5}Zn_{0.5}Fe_2O_4$) on the magnetic properties and reported that the $BaTiO_3$-$CoFe_2O_4$ composites enhance magnetoresistance and magnetocapacitance effects, which were dependent on the percentage of ferrite [20]. There are a few works that study $NiTiO_3$ ilmenite ceramic, to synthesize the composite and study the effect of magnetic phase on the optical and ferroelectric properties. Ansari et al. synthesized $NiTiO_3$-$NiFe_2O_4$ composites by a sol-gel combustion route with onion extract used as a fuel [21], and reported that the $NiTiO_3$-$NiFe_2O_4$ nanocomposites showed superparamagnetic behavior with saturation magnetization (M_s) of 6 emu/g and coercive field (H_c) and remanent magnetization (M_r) approximately equal to 0. This work supported a green method to prepare $NiTiO_3$ composites. Nevertheless, this work has not investigated the optical and ferroelectric properties of composites. As per our knowledge, no information on optical, ferroelectric, and ferromagnetic characteristics of $NiTiO_3$-$MnFe_2O_4$ composites are available in the literature. In this work, we have reported a simple method to prepare the $NiTiO_3$-$MnFe_2O_4$ composites. Optical, ferroelectric, and magnetic characterizations of prepared composites were systematically carried out.

2. Experiment

2.1. Materials

Monohydrate citric acid ($C_6H_8O_7{\cdot}H_2O$) was purchased from Guangdong Xilong Chemical Co., China. Nickel (II) nitrate hexahydrate ($Ni(NO_3)_2{\cdot}6H_2O$), iron (III) nitrate nonahydrate ($Fe(NO_3)_3{\cdot}9H_2O$), manganese (II) chloride tetrahydrate ($MnCl_2{\cdot}4H_2O$) and tetraisopropoxytitanium ($Ti[OCH(CH_3)]_4$) were purchased from Sigma Aldrich and used without further purification.

2.2. Sample preparation

The $(1-x)NiTiO_3$-$xMnFe_2O_4$ (where x = 0, 0.05 and 0.10) composites were synthesized by a sol-gel method and referred to as NTO-yMFO, where y stands for $MnFe_2O_4$(MFO) content. Citric acid solution was used as a solvent and a chelating agent. First, citric acid was dissolved into distilled water to make a solution with molar concentration of 1.5 M. Tetraisopropoxytitanium (TTIP) was dropped into the above solution under vigorous stirring for about 1 h at 70°C. After that, nickel nitrate was introduced into the solution and the mixed solution was kept stirring for around 1 h. Then, iron nitrate and manganese chloride were added with appropriate molar portions of metal nitrates fixed at Mn:Fe ratio of 1:2. The solutions were continuously stirred at 70°C until a gel was formed. The gel precursor was dried at 100°C for a day to remove excess water and turned into a foam block of xerogel. The xerogel was heated at 400°C for 2 h and annealed at 800°C in air for 3 h with a heating rate of 10°C/min. After cooling to room temperature, it was ground in an agate mortar to obtain composite powders. The overall synthesis procedure of $(1-x)NiTiO_3$-$xMnFe_2O_4$ composite samples is schematically represented in Figure 1.

For *P-E* loop measurement, $(1-x)NiTiO_3$-$xMnFe_2O_4$ composite powders were well mixed

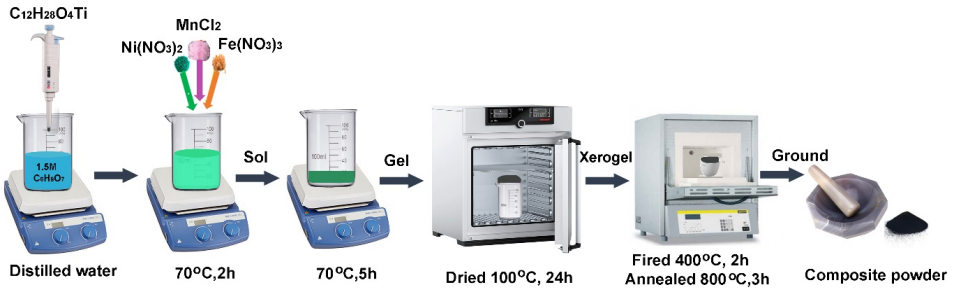

Fig. 1. Schematic diagram of the sol-gel method to synthesized $(1-x)NiTiO_3$-$xMnFe_2O_4$ composites

with 3 wt.% polyvinyl alcohol (PVA, 5%) and then uniaxially pressed into a disc with a diameter of 10 mm and $\sim$ 1 mm under pressure of 150 MPa. The pressed pellets were sintered at 1200°C with a heating and a cooling rate of 5°C/ min in air for 5 h in a box furnace. After sintering, the sintered pellets were polished, cleaned, and a silver electrode was deposited on both sides of the pellet.

2.3. Characterization

X-ray diffraction (XRD) pattern was measured by an X-ray diffractometer (Philips- X'PertPro) using Cu Kα (λ = 1.54056 Å) radiation. The Raman spectra were employed by a micro Raman spectrophotometer (JASCO Raman NRS-3000). Microstructure of the samples was observed by scanning electron microscopy (Tabletop Microscope HITACHI TM4000Plus) with acceleration voltage of 15 kV. The room temperature optical reflectance data of the synthesized samples were investigated using a UV–Vis Spectrometer (JASCO V- 750). Ferroelectric hysteresis loops (P–E) were tested by a ferroelectric tester (Radiant Precision Premier II). The magnetic properties of the $NiTiO_3$ and $(1-x)NiTiO_3$-$xMnFe_2O_4$ composites were recorded at room temperature in range of -10 kOe $\leq H \leq$ 10 kOe by a vibrating sample magnetometer (Lakeshore 7400).

3. Results and discussion

3.1. Structural analysis

Figure 2 depicts the XRD patterns of synthesized $(1-x)NiTiO_3$-$xMnFe_2O_4$ (x = 0, 0.05 and 0.10) composites annealed at 800°C for 3 h. All samples included the observed diffraction peaks at 2θ = 24.03, 33.16, 35.72, 40.76, 49.54, 53.90, 57.35, 62.35, and 64.06, which corresponds to the (hkl) lattice planes of (012), (104), (110), (113), (024), (116), (018), (124), and (300), respectively. It belongs to the rhombohedral structure with R $\bar{3}$ space group of $NiTiO_3$ structure. The observed peaks and corresponding planes are well matched with standard JCPDS 33-0960. It is noted that the expected diffraction peaks of MFO in composite materials can be detected diffraction peaks at 2θ = 30.31, 37.32 which exhibited a cubic spinel crystal structure with space group Fdm$\bar{3}$ (JCPDS card number 74-2403). The relative intensity of the $MnFe_2O_4$ diffraction varied corresponding to the $MnFe_2O_4$ content. The X-ray diffraction spectra of the synthesized powders indicated that mixed crystalline spinel–ilmenite phases have been formed without any trace of foreign phases. These results exhibited the successful formation of the NTO and MFO crystal phases in the composites, and no prominent chemical reactions happened during the synthesis process, which obtained the individual separation of ferroelectric and ferromagnetic phases. Rietveld refinement was carried out for analysis of crystal structure. For refinement work, constituent information phases were used from the crystallography open database. The refined crystal parameters of the constituent phases and their composites are shown in Table 1. The presence of both phases in composites has not influenced the crystal structure of the individual phase, showing that no additional chemical interactions between ferroelectric and ferromagnetic phases form the impurity

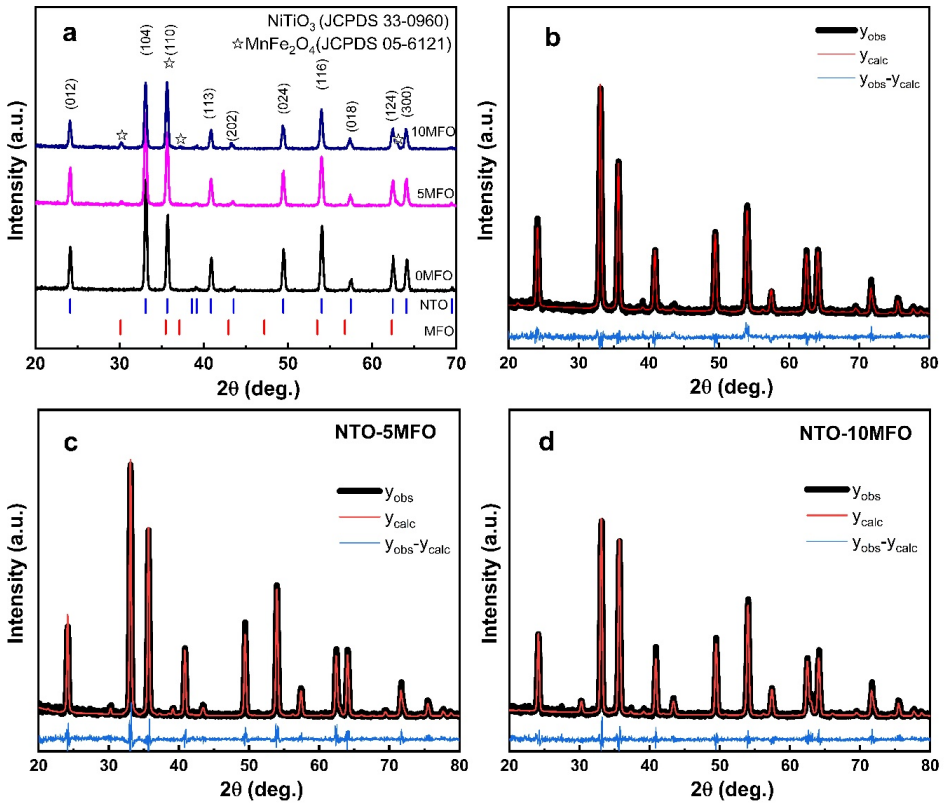

Fig. 2. XRD pattern of a) $(1-x)NiTiO_3$-$xMnFe_2O_4$ composites and b-d) Rietveld refinement analysis

Table 1. Lattice parameters and crystalline size of $(1-x)NiTiO_3$-$xMnFe_2O_4$ composites

Sample	Lattice parameters			Unit cell volume (Å^3)		Crystalline size (nm)		R_{wp} %
	NTO		MFO	NTO	MFO	NTO	MFO	
	a (Å)	c (Å)	a (Å)	phase	phase	phase	phase	
NTO	5.0284	13.7912	–	301.98	–	35	–	17.6
NTO-5MFO	5.0285	13.7916	8.3373	302.00	579.53	37	26	18.7
NTO-10MFO	5.0343	13.8074	8.3341	303.04	578.86	38	27	18.3

phase and and that their symmetry is maintained in the synthesized composite materials. Moreover, the addition of $MnFe_2O_4$ phase resulted in a slight change in lattice parameters of $NiTiO_3$ phase. The a and c lattice constants of $NiTiO_3$ increase slightly with an increase of $MnFe_2O_4$ content. Further, the a lattice constant of MFO had the opposite trend to the lattice constant of $NiTiO_3$. The addition of MFO caused an expansion of NTO lattice that induced strain, which can affect the electrical characteristics of the composite samples. It can be clearly seen that the diffraction peak intensity of the MFO phase increased with the increasing of MFO concentration, which confirmed the two phases coexisted in composites. The cell volume of NTO phase increased with an increase of MFO content. The increasing of unit cell volume of NTO can be ascribed to the expansion strain of the NTO phase. In contrast, the cell volume of the MFO phase increased, which means that the MFO lattice was expanded. The strain formation can be one of the critical parameters which influence the optical, electric, and magnetic properties of composite samples.

3.2. Raman analysis

Figure 3 shows the Lorentzian deconvoluted Raman spectra of $(1-x)NiTiO_3$-$xMnFe_2O_4$ composites monitored in the range of 150-1000 cm^{-1} at room temperature. The pristine $NiTiO_3$ presented ten Raman active modes ($5A_g$ + $5E_g$) of ilmenite structure, which are in agreement with reports in the literature [22]. However, the intensity of these vibration modes of Raman signals of composite samples showed the breadth of Raman modes. These results were due to the overlapping of Raman modes of MFO with vibration modes of ilmenite structure. The intensity of Raman modes of MFO was very weak in comparison with those of vibration modes in $NiTiO_3$ material. Therefore, these vibration modes were not observed clearly in Raman spectra.

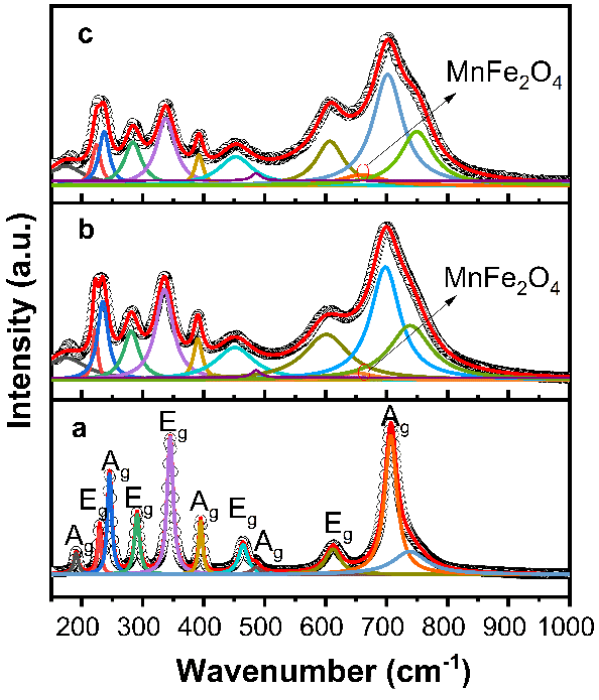

Fig. 3. Raman spectra of a) NTO, b) NTO-5MFO and c) NTO-10MFO composites

However, the overlapping of the Raman vibration modes of both phases caused the broadening Raman vibration modes. We can observe these modes by deconvolution of the Raman spectrum of the composite samples. Lorentzian least square fitting was used to fit the experimental data to analyze the line width. Ten Raman vibration modes corresponding to pure $NiTiO_3$ materials were observed from the fitting curves. In addition, the Raman vibration mode of $MnFe_2O_4$ at 653 cm^{-1} was observed in the Raman spectra due to the symmetric stretching of oxygen atoms along Fe–O bonds in the tetrahedral sites in $MnFe_2O_4$ material [23]. The intensity of the Raman vibration band of MFO phase increased with an increase of MFO content, which revealed the MFO phase existed in the synthesized samples. No modes of impurity phase were detected from Raman spectra, which indicated the high purity of the prepared composite samples.

3.3. Surface morphology

The SEM images of the $(1-x)NiTiO_3$-$xMnFe_2O_4$ ceramics are presented in Figure 4. All images show remarkably clear boundaries; however, the grain size is not homogeneous and grains are in a wide range of size distribution. The average grain size of the samples was estimated using IMAGE-J software [24]. It is clear from the figures that the pure $NiTiO_3$ samples have smaller grains and more pore in comparison with composite samples. The average grain size of pure sample is about 3.7 μm. It increases to 4.7 μm and 5.0 μm for composite samples with 5 and 10 mol. % $MnFe_2O_4$, respectively. Moreover, the pores decrease with introducing $MnFe_2O_4$. The addition of $MnFe_2O_4$ phase in $NiTiO_3$ material can work as a sintering aid, which increases the rate of diffusion and enhances the performance of the densifying mechanism.

3.4. Optical properties

The optical properties of synthesized $(1-x)NiTiO_3$-$xMnFe_2O_4$ composite powders were studied by UV–Vis diffuse reflectance spectra, which is presented in Figure 5. The color of $(1-x)NiTiO_3$-$xMnFe_2O_4$ composites changed from the light yellow color of pure $NiTiO_3$ to the black color of $NiTiO_3$-$MnFe_2O_4$ composites. The absorption spectrum of $NiTiO_3$ showed two main absorption regions: 300 nm – 550 nm (the transition $^3A_{2g}(3F) \rightarrow {}^3T_{1g}(3P)$) and 650 nm – 900 nm (the transition $^3A_{2g}(3F) \rightarrow {}^3T_{1g}(3F)$) [25, 26]. The op-

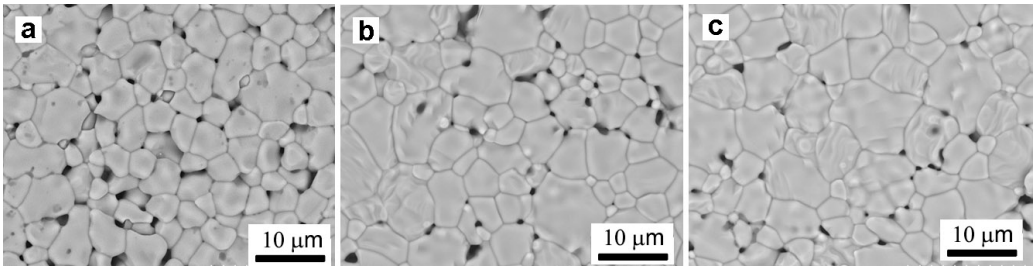

Fig. 4. SEM images of a) NTO, b) NTO-5MFO and c) NTO-10MFO composites

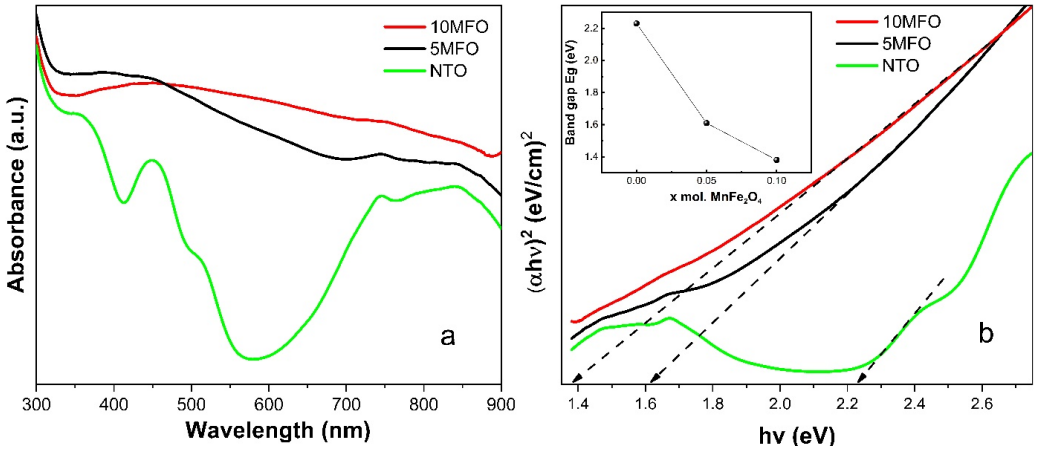

Fig. 5. a) Optical absorbance spectra and b) plotting of $(\alpha h\nu)^2$ versus photon energy of $(1-x)NiTiO_3$-$xMnFe_2O_4$ composites

tical absorption of $NiTiO_3$-$MnFe_2O_4$ composites exhibited a broad band in 300 nm – 550 nm region, which indicates that the band edge absorption has been extended to the visible light region when the $MnFe_2O_4$ was introduced into $NiTiO_3$ to form composites. The optical band gap was estimated using the Wood-Tauc method [27]. The optical absorption of materials was presented by equation $(\alpha h\nu) \sim (h\nu\text{-}E_g)^n$, where α is the linear absorbance coefficient, $h\nu$ is the photon energy, E_g is the optical band gap energy, and n is a constant which relates to different types of electronic transition (n = 2 and 1/2 for an indirect and direct bandgap material). The plot of $(\alpha h\nu)^2$ as a function of photon energy $(h\nu)$ of the synthesized powders was exhibited in Figure 5b. The optical band gap values were determined by extrapolating the linear portion of $(\alpha h\nu)^2$ versus $h\nu$ plot to the point at $(\alpha h\nu)^2$ = 0 [28]. The relationship between bandgap energy and MFO content is illustrated in the inset of Figure 5b. The E_g value decreased with an increase of MFO content. It decreased from 2.23 eV to 1.38 eV for pure $NiTiO_3$ and $NiTiO_3$-$MnFe_2O_4$ composites with 10 mol.% MFO, respectively. These results revealed that the optical bandgap of $NiTiO_3$ were significantly changed by the $MnFe_2O_4$ phase. The bandgap energy of $MnFe_2O_4$ material is narrower than that of $NiTiO_3$ and this could result in decreasing the band gap value of the composites. The decrease of bandgap values of host materials due to ferrite phase is in agreement with the results which reported from previous studies [29, 30]. Moreover, there are many other factors that can be responsible for decreasing bandgap energy, such as strain, grain size effect, etc. [31, 32]. This result indicated the ability to modify the optical bandgap value by simple manipulation of the MFO content.

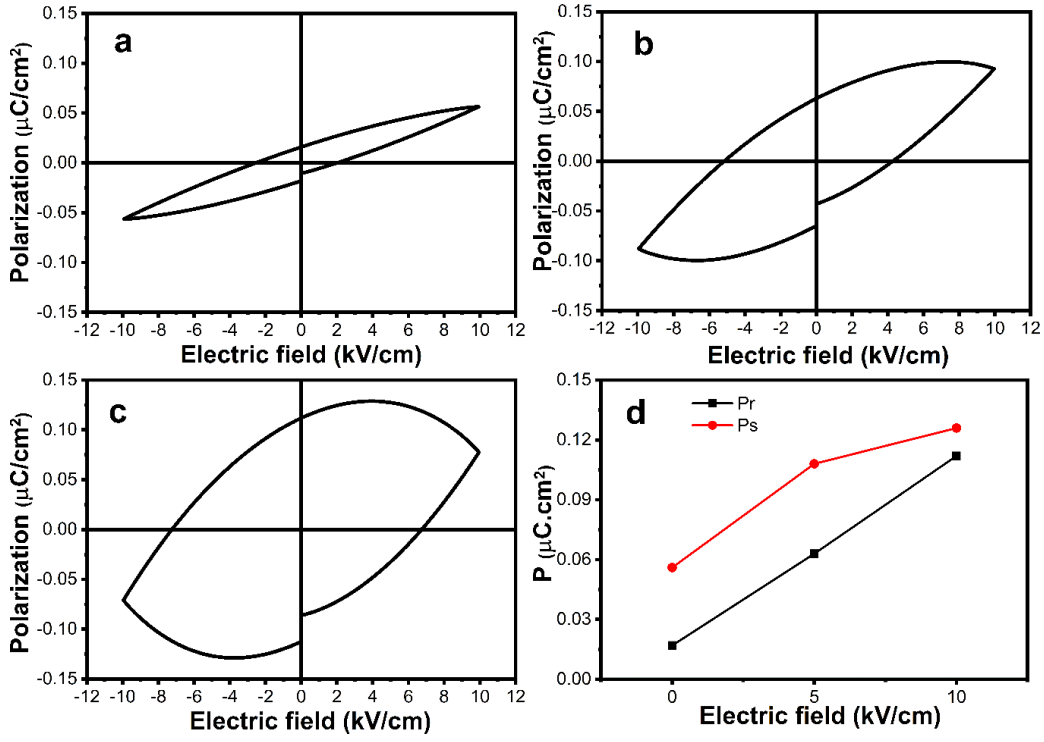

Fig. 6. Ferroelectric loops of a) NTO, b) NTO-5MFO, c) NTO-10MFO composites and d) dependence of P_s and P_r of composites on MFO content

3.5. Ferroelectric properties

The ferroelectric properties of prepared samples have been determined from the *P-E* loop recorded at room temperature under the constant field of 10 kV/cm, which is shown in Figure 6a-d. The *P-E* loops of prepared samples showed a typical *P-E* loop, indicating the ferroelectric properties of these samples. However, the shape of *P-E* loops depended on the ratios of phases between ferroelectric phase and ferrite phase. The pure $NiTiO_3$ without ferrite phase exhibited a small hysteresis loop. Increasing the ferrite phase to 5%, the *P-E* loop of this sample is well saturated with the calculated values of remanent polarization ($+P_r$) of 0.063 μC/cm^2 and saturation polarization ($+P_s$) of 0.108 μC/cm^2. These values are higher than those of the pure $NiTiO_3$ sample with remanent polarization ($+P_r$) of 0.017 μC/cm^2 and saturation polarization ($+P_s$) of 0.056 μC/cm^2.

It showed that both saturation and remanent polarization values of synthesized composites increased with an increase of ferrite content. The value of P_s increased with $MnFe_2O_4$ content, which could be related to the space charge contribution of the ferrite phase [33]. The addition of a magnetic phase into a ferroelectric phase generally caused ferroelectric properties to decline because the presence of the ferromagnetic phase resulted in a leakage current in the composite, consequently the ferroelectric properties of the composite decreased [34, 35]. However, the addition of the ferromagnetic phase in the ferroelectric material can enhance the ferroelectricity at certain content due to attribution of coherent interfaces. The ferroelectric properties rise when ferroelectric content increases to a threshold [36]. In our work, we observed that ferroelectric properties increased at 5% $MnFe_2O_4$ content. However, the lossy current occurred with decreasing of polarization at a high electric field when $MnFe_2O_4$ content was 10%. An increase of coercivity value and a round-shaped *P-E* loop at high MFO content can be attributed to higher loss and a rise in conductivity in the composites [30, 36]. Our

results showed similar trends with some other system composites of the ferroelectric and ferromagnetic phase reported in the literature, such as $Na_{0.5}Bi_{0.5}TiO_3$ – $BaFe_{12}O_{19}$ [33], $CoFe_2O_4$-$Pb0_{.7}Ca_{0.3}TiO_3$ [37]. Sharma et al. observed that ferroelectric behaviors of $CoFe_2O_4$-$Pb_{0.7}Ca_{0.3}TiO_3$ composites at room temperature were strongly dependent on ferrite concentration [37]. The polarization value of $CoFe_2O_4$-$Pb_{0.7}Ca_{0.3}TiO_3$ composite increased with the increasing of ferrite content. Pattanayak et al. showed that the values of saturation polarization and remanent polarization of $Na_{0.5}Bi_{0.5}TiO_3$-$BaFe_{12}O_{19}$ composites increased with $BaFe_{12}O_{19}$ content up to 30 wt.% and then dramatically decreased because of an increase of leakage current through ferrite paths [33]. Jain et al. reported on the ferroelectric and magnetic properties of $Ba_{0.83}Ca_{0.10}Sr_{0.07}TiO_3$-$MnFe_2O_4$ multiferroic composites [19]. $Ba_{0.83}Ca_{0.10}Sr_{0.07}TiO_3$ material showed a ferrimagnetic hysteresis loop with considerable saturation magnetization; however, it exhibited a slight reduction in dielectric and ferroelectric with $MnFe_2O_4$ addition [19].

Figure 7 shows the leakage current of pristine $NiTiO_3$ and $(1-x)NiTiO_3$-$xMnFe_2O_4$ composites as a function of an applied electric field. The leakage current of all samples increased with the increasing of an applied field. The increment of leakage current versus rising of the electric field is non-

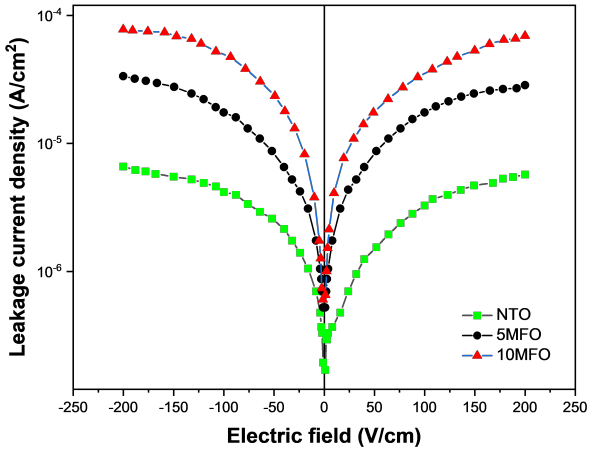

Fig. 7. Leakage current density vs. electric field of $NiTiO_3$ and $(1-x)NiTiO_3$-$xMnFe_2O_4$ composites

linear, which suggested non-Ohmic characteristic of this system. In addition, it also increased with increasing of $MnFe_2O_4$ content. The result may be due to the attribution of lower resistive $MnFe_2O_4$ material in a higher resistive $NiTiO_3$ phase.

3.6. Magnetic properties

Figure 8 showed the magnetization vs. magnetic field hysteresis loops for the spinel–ilmenite $(1-x)NiTiO_3$-$xMnFe_2O_4$ composite samples at room temperature. The pure $NiTiO_3$ consisted of paramagnetic materials, which is consistent with reports in the literature [5]. The loops of $NiTiO_3$-$MnFe_2O_4$ composites clearly exhibited the existence of an ordered magnetic structure in the ilmenite-ferrite composite. Magnetic parameters of synthesized composites are presented in Table 2. The magnetic behavior of $(1-x)NiTiO_3$-$xMnFe_2O_4$ composites showed similar behavior, with a clear S-shaped ferromagnetic hysteresis loop. The magnetic saturation magnetization (M_s), remanent magnetization (M_r), and coercive field (H_c) of the composites have a strong dependence on the addition of the MFO. As the analysis in the XRD above, results implied that the $MnFe_2O_4$ ferrite phase formed in the composite samples, which explained why the magnetic properties of these samples were enhanced and exhibited the ferromagnetic behavior. The increase in magnetic properties of synthesized composites is expected because magnetic properties of composites depend on the ferrite amount added into composites. The remanent and saturation magnetization increased with an increase of MFO content, which indicated a significant increase in magnetic characteristics with the MFO addition in NTO. The addition of MFO phase resulted in an increase of M_s and M_r, which play a crucial role in determining the magnetization of synthesized composites because $NiTiO_3$ is a nonmagnetic material. The higher saturation magnetization in composite samples with higher MFO content could be explained by the individual ferrite grain distribution in composite, which acts as a center of the magnetization and the saturation magnetization of the composites is the vector sum of these individual contributions. The clear

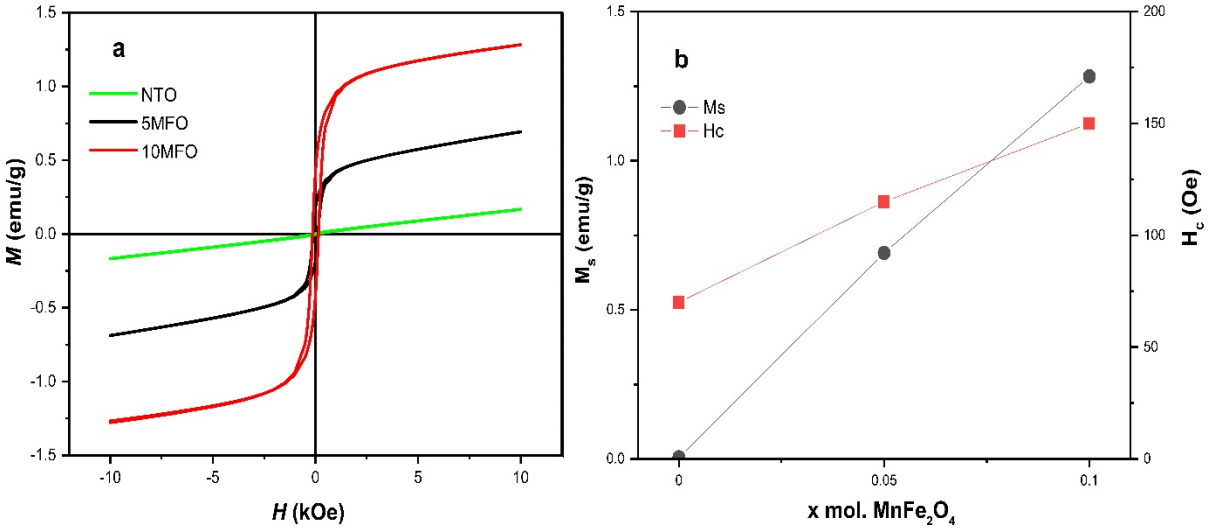

Fig. 8. a) Magnetic hysteresis loops of the $(1-x)NiTiO_3$-$xMnFe_2O_4$ nanocomposite samples measured at room temperature and b) dependence of M_s and M_r of composites on MFO content

Table 2. Magnetic parameters of $(1-x)NiTiO_3$-$xMnFe_2O_4$ composites

Samples	Magnetic Saturation (emu/g)	Remanent magnetization (emu/g)	Coercivity (Oe)	Remanent Ratio M_r/M_s
0	0.005	0.0001	70	0.02
$x = 5\%$	0.691	0.174	135	0.252
$x = 10\%$	1.283	0.417	150	0.325

P–E and *M–H* hysteresis loops of the synthesized composite samples showed that both ferroic properties in $(1-x)NiTiO_3$-$xMnFe_2O_4$ composites existed at room temperature.

4. Conclusions

In this work, we reported the synthesis of $NiTiO_3$-$MnFe_2O_4$ nanocomposites with a one-step sol-gel method. The XRD confirmed the formation of mixed phases of ilmenite $NiTiO_3$ and spinel $MnFe_2O_4$. The optical bandgap value of composites decreased with an increase of $MnFe_2O_4$ content. The composites exhibited both ferroelectric and magnetic behaviors at room temperature. There is a significant increase in magnetic qualities with the existence of spinel $MnFe_2O_4$ in $NiTiO_3$ ceramics. Magnetic studies exhibited the formation of ferromagnetic hysteresis loops with saturation magnetization for all composite samples. This research showed a simple approach to synthesize mixed phases of ilmenite $NiTiO_3$ and spinel $MnFe_2O_4$ materials to modify optical properties and to enhance ferroelectric and magnetic properties, which could be applied in development of multifunction materials.

Acknowledgements

This research is funded by the Vietnam Ministry of Education and Training under Grant number B2021-BKA-2.

References

[1] Hill NA. Why Are There so Few Magnetic Ferroelectrics. *J Phys Chem B.* 2000;104:6694–6709.

[2] Alam M, Talukdar S, Mandal K. Multiferroic properties of bilayered $BiFeO_3/CoFe_2O_4$ nano-hollowspheres. *Mater Lett.* 2018;210:80–3.

[3] Nan CW, Bichurin MI, Dong S, Viehland D, Srinivasan G. Multiferroic magnetoelectric composites: Historical perspective, status, and future directions. *J Appl Phys.* 2008;103(3).

[4] Ruiz-Preciado MA, Kassiba A, Gibaud A, Morales-

Acevedo A. Comparison of nickel titanate ($NiTiO_3$) powders synthesized by sol-gel and solid state reaction. *Mater Sci Semicond Process.* 2015;37:171–8.

[5] Heller GS, Stickler JJ, Kern S, Wold A. Antiferromagnetism in $NiTiO_3$. *J Appl Phys.* 1963;34(4):1033.

[6] Thang P Van, Dung DD, Bac LH, Hung PP, Ngoc TVD. Structural, Optical, Ferroelectric and Magnetic Properties of $NiTiO_3$ Ceramic Synthesized by Citrate Gel Method. *Int J Nanosci.* 2021;20(1):1–7.

[7] Acharya T, Choudhary RNP. Structural, Ferroelectric, and Electrical Properties of $NiTiO_3$ Ceramic. *J Electron Mater.* 2015;44(1):271–80.

[8] Tursun R, Su Y, Yu Q, Tan J. Room-temperature coexistence of electric and magnetic orders in $NiTiO_3$ and e ff ect of ethylene glycol. *Mater Sci Eng B.* 2018;228 (November 2017):96–102.

[9] Hung PP, Dung DD, Tuan NH, Trung NN, Bac LH. Iron induced room temperature ferromagnetism in ilmenite $NiTiO_3$ materials. *Mater Lett.* 2017;209(33):284–6.

[10] Tursun R, Su YC, Yu QS, Tan J, Hu T, Luo ZB, et al. Effect of doping on the structural, magnetic, and ferroelectric properties of $Ni_{1-x}A_xTiO_3$ (A = Mn, Fe, Co, Cu, Zn; x = 0, 0.05, and 0.1). *J Alloys Compd.* 2019;773:288–98.

[11] Lenin N, Karthik A, Sridharpanday M, Selvam M, Srither SR, Arunmetha S, et al. Electrical and magnetic behavior of iron doped nickel titanate ($Fe^{3+}/NiTiO_3$) magnetic nanoparticles. *J Magn Magn Mater.* 2016;397:281–6.

[12] Popa M, Bruna P, Crespo D, Calderon Moreno JM. Single-phase $MnFe_2O_4$ powders obtained by the polymerized complex method. *J Am Ceram Soc.* 2008;91(8):2488–94.

[13] Chinnasamy CN, Narayanasamy A, Ponpandian N, Chattopadhyay K, Shinoda K, Jeyadevan B, et al. Mixed spinel structure in nanocrystalline $NiFe_2O_4$. *Phys Rev B – Condens Matter Mater Phys.* 2001;63(18):2–7.

[14] Rajalakshmi R, Remya KP, Viswanathan C, Ponpandian N. Enhanced electrochemical activities of morphologically tuned $MnFe_2O_4$ nanoneedles and nanoparticles integrated on reduced graphene oxide for highly efficient supercapacitor electrodes. *Nanoscale Adv.* 2021;3(10):2887–901.

[15] Baig MM, Yousuf MA, Agboola PO, Khan MA, Shakir I, Warsi MF. Optimization of different wet chemical routes and phase evolution studies of $MnFe_2O_4$ nanoparticles. *Ceram Int.* 2019;45(10):12682–90.

[16] Atif M, Nadeem M, Khalid W, Ali Z. Structural, magnetic and impedance spectroscopy analysis of $(0.7)CoFe_2O_4+(0.3)BaTiO_3$ magnetoelectric composite. *Mater Res Bull.* 2018;107(May):171–9.

[17] Grigalaitis R, Vijatović Petrović MM, Bobić JD, Dzunuzovic A, Sobiestianskas R, Brilingas A, et al. Dielectric and magnetic properties of $BaTiO_3$-$NiFe_2O_4$ multiferroic composites. *Ceram Int.* 2014;40(4):6165–70.

[18] Remya KP, Rajalakshmi R, Ponpandian N. Development of $BiFeO_3/MnFe_2O_4$ferrite nanocomposites with enhanced magnetic and electrical properties. *Nanoscale Adv.* 2020;2(7):2968–76.

[19] Jain A, Wang YG, Wang N, Li Y, Wang FL. Tuning the dielectric, ferroelectric and electromechanical properties of $Ba_{0.83}Ca_{0.10}Sr_{0.07}TiO_3$-$MnFe_2O_4$ multiferroic composites. *Ceram Int.* 2020;46(6):7576–85.

[20] Pachari S, Pratihar SK, Nayak BB. Enhanced magnetocapacitance response in $BaTiO_3$–ferrite composite systems. *RSC Adv.* 2015;5(128):105609–17.

[21] Ansari F, Bazarganipour M, Salavati-Niasari M. $NiTiO_3/NiFe_2O_4$ nanocomposites: Simple sol-gel autocombustion synthesis and characterization by utilizing onion extract as a novel fuel and green capping agent. *Mater Sci Semicond Process.* 2016;43:34–40.

[22] Bellam JB, Ruiz-Preciado MA, Edely M, Szade J, Kassiba AJ and AH. Visible-light photocatalytic activity of nitrogen-doped $NiTiO_3$ thin films prepared by a co-sputtering process. *R Soc Chem.* 2015;5:10551–9.

[23] Amulya MAS, Nagaswarupa HP, Kumar MRA, Ravikumar CR, Kusuma KB. Sonochemical synthesis of $MnFe_2O_4$ nanoparticles and their electrochemical and photocatalytic properties. *J Phys Chem Solids.* 2021;148(July 2020):109661.

[24] Schneider CA, Rasband WS, Eliceiri KW. NIH Image to ImageJ: 25 years of image analysis. *Nat Methods.* 2012;9(7):671–5.

[25] Rossman GR, Shannon RD, Waring RK. Origin of the yellow color of complex nickel oxides. *J Solid State Chem.* 1981;39(3):277–87.

[26] Llusar M, García E, García MT, Esteve V, Gargori C, Monrós G. Synthesis and coloring performance of Ni-geikielite (Ni,Mg)TiO_3 yellow pigments: Effect of temperature, Ni-doping and synthesis method. *J Eur Ceram Soc.* 2015;35(13):3721–34.

[27] Wood DL, Tauc J. Weak Absorption Tails in Amorphous Semiconductors. *Phys Rev B.* 1972 Apr 15;5(8):3144–51.

[28] Madhan K, Murugaraj R. Investigation on Microstructural, Electrical and Optical Properties of Nd-Doped $BaCo_{0.01}Ti_{0.99}O_3$ Perovskite. *J Electron Mater.* 2020;49(1):377–84.

[29] Wang X, Jiang L, Li K, Wang J, Fang D, Zhang Y, et al. Fabrication of novel Z-scheme $SrTiO_3/MnFe_2O_4$ system with double-response activity for simultaneous microwave-induced and photocatalytic degradation of tetracycline and mechanism insight. *Chem Eng J.* 2020;400(February):125981.

[30] Chinnathambi A, Nasif O, Alharbi SA, Khan SS. Enhanced optoelectronic properties of multifunctional $MnFe_2O_4$ nanorods decorated Co_3O_4 nanoheterostructure: Photocatalytic activity and antibacterial behavior. *Mater Sci Semicond Process.* 2021;134(May):105992.

[31] Ramana C V., Smith RJ, Hussain OM. Grain size effects on the optical characteristics of pulsed-laser deposited vanadium oxide thin films. *Phys Status Solidi Appl Res.* 2003;199(1):5–7.

[32] Singh DJ, Xu Q, Ong KP. Strain effects on the band

gap and optical properties of perovskite $SrSnO_3$ and $BaSnO_3$. *Appl Phys Lett.* 2014;104(1):1–5.

[33] Pattanayak R, Raut S, Kuila S, Chandrasekhar M, Panigrahi S. Multiferroism of [$Na_{0.5}Bi_{0.5}TiO_3$ – $BaFe_{12}O_{19}$] lead-free novel composite systems. *Mater Lett.* 2017;209:280–3.

[34] Devan RS, Deshpande SB, Chougule BK. Ferroelectric and ferromagnetic properties of (x)$BaTiO_3$+(1-x)$Ni_{0.94}Co_{0.01}Cu_{0.05}Fe_2O_4$ composite. *J Phys D Appl Phys.* 2007;40:1864–8.

[35] Manjusha, Rawat M, Yadav KL. Structural, dielectric, ferroelectric and magnetic properties of (x) $CoFe_2O_4$-(1-x)$BaTiO_3$ composite. *IEEE Trans Dielectr Electr Insul.* 2015;22(3):1462–9.

[36] Zhang H, Ke H, Zhang L, Wang W, Jia D, Miao P, et al. Ferroelectric properties of magnetoelectric $CoFe_2O_4/Bi_{3.15}Nd_{0.85}Ti_3O_{12}$ composite ceramics with coherent-lattice interfaces. *Scr Mater.* 2017;127:29–32.

[37] Sharma A, Kotnala RK, Negi NS. Observation of multiferroic properties and magnetoelectric effect in (x)$CoFe_2O_4$-(1-x)$Pb_{0.7}Ca_{0.3}TiO_3$ composites. *J Alloys Compd.* 2014;582:628–34.

Received 2022-12-03
Accepted 2023-01-31